ChemPubSoc Europe

DOI: 10.1002/cplu.201800539

CHEMPLUSCHEM Full Papers

Assembling All-Solid-State Lithium–Sulfur Batteries with Li_3N-Protected Anodes

Abdulkadir Kızılaslan* and Hatem Akbulut[a]

The construction of all-solid-state batteries is now easier after the successful synthesis of sulfur-based solid electrolytes with extremely high ionic conductivities. Utilizing lithium metal as the anode in these batteries requires a protective solid electrolyte layer to prevent corrosion due to the highly reactive nature of lithium. Li_3N coating on lithium metal is a promising way of preventing the degradation of the electrolyte during charge and discharge. In this study, utilization of a Li_3N-coated lithium anode and $Li_7P_3S_{11}$ solid electrolyte are reported, where a quaternary reduced graphene oxide (rGO)/S/carbon black/$Li_7P_3S_{11}$ composite is used as cathode in the assembled cell. Our results indicate that protecting the Li metal with a Li_3N coating does not affect the electrochemical characteristics of the cell and extends the cycle life of the battery. A cell assembled with a protective layer was shown to having 306 mAh g^{-1} capacity after 120 cycles at 160 mAh g^{-1} current density, whereas a cell without protective layer had a capacity of 260 mAh g^{-1}.

Introduction

Challenging environmental problems arising from the use of fossil fuels urge the world to use environmentally friendly power sources. Lithium ion batteries (LIBs) are considered the most prominent alternatives to replace the use of fossil fuels on vehicles. Yet several concerns have to be eliminated before the adoption of these batteries into vehicles. Current LIBs utilizing ether based liquid electrolytes to shuttle lithium ions between anode and cathode. Flammability risk of these ether based liquid electrolytes has to be taken more into consideration as we scale up the LIBs from the ones used in electronic devices into vehicles. Besides, LIBs should supply more power density to be employed in vehicles due to economic concerns. Solid electrolytes are now the most favourable alternatives to replace liquid electrolytes especially after the successful synthesis of sulfide electrolytes having lithium ion conductivity on the order or up of commercial ether based liquid electrolytes.

Sulfidic solid electrolytes are synthesized broadly in three forms. LMPS(M=Ge,Sn,Si) type solidelectrolytes are synthesized in tetragonal crystal structures and reported to having ionic conductivity of 12 mS cm^{-1} and 4 mS cm^{-1} for $Li_{10}GeP_2S_{12}$ and $Li_{10}SnP_2S_{12}$, respectively.[1,2] Subsequent syntheses focused on doping halogens into the structure resulted better electrochemical window up to 8 V (vs Li/Li^+). Structures in Li_6PS_5X (X=Cl,Br,I) formula are having cubic argyrodite crystal structure with ionic conductivities barely less than LMPS type electrolytes but still on the order of 10^{-3} S cm^{-1}.[3] Lastly, solid electrolytes in (x)Li_2S-(100-x)P_2S_5 system where x=67,70,75 and 80 yields superionic conductor solid electrolytes with ionic conductivity of the range 1–10 mS cm^{-1}. Among those structures, extremely high ionic conductivities reported on the 70Li_2S:30P_2S_5 system with 16 mS cm^{-1}.[4]

Although great strides have been achieved in conductivity front, main challenge left to be overcome is to construct compatible anode and cathode pairs with the synthesized solid electrolytes. Wenzel et al[5] reported the instability of LMPS type solid electrolytes along with the phases formed at interface utilizing XPS analysis. A stable solid electrolyte interface has to be composed of phases that are electronically(ionically) insulating (conducting). Yet the phases formed on LMPS type solid electrolytes are reported to having electronically conductive phases in the form of Li_xM_y. Such type of interfaces would consume anodes, through reducing electrolytes, and eventually kill the battery.

Increasing number of studies has focused on the engineering of the electrode-electrolyte interfaces to get compatible pairs specially to utilize lithium as anode. Ab Initio Molecular Dynamic (AIMD) studies based on Density Functional theory (DFT) are very effective and powerful way of searching desired systems over a large system database. Zhu et al.[6] searched different binary and ternary fluorides, sulfides, oxides and nitrides that are stable against Li anode. They concluded that most nitride structures behave cathodic against Li metal. Intentional modification of Li anode surface before assembling the cell is one plausible way to eliminate the adverse side effects of SEI layer. This layer would not only prevent the aforementioned phase problems but also construct better wetted interface. Moreover the common problem of Li anode dendritic growth may also be suppressed with the formation of proper coatings on the anode.

Based on nitride structures to be coated onto the Li metal, Li_3N having two common polymorphs (α-Li_3N and β-Li_3N) already known as exhibiting high Li^+ ionic conductivities.Several studies were successfully conducted to coat Li_3N layer on the Li anode and encouraging results showing less impedance

[a] A. Kızılaslan, Prof. H. Akbulut
Metallurgy and Materials Science Department
Sakarya University
Esentepe Campus, 54050 Sakarya (Turkey)
E-mail: akizilaslan@sakarya.edu.tr
akbulut@sakarya.edu.tr

Supporting information for this article is available on the WWW under https://doi.org/10.1002/cplu.201800539

on the interface are obtained.[7–11] Besides, coating Li_3N onto the Li metal surface can be accomplished via the direct nitridation of Li metal with N_2 gas at room temperature. Contrary to other more expensive and time consuming thin film coating processes, direct nitridation is a very effective way of utilizing the highly reactive nature of lithium.

On the cathode side sulfur is one of the promising materials with its theoretical energy density of 2600 $Wh\,kg^{-1}$ and is already at the focus of Li–S batteries with liquid electrolytes. However, the formation and shuttle of lithium polysulfides formed on these systems are still challenging to be overcome in Li–S batteries with liquid electrolytes. Solid electrolytes are now the most exciting alternatives to replace liquid electrolytes. In all solid state lithium ion batteries (ASSLIBs), one has to composite sulfur with a conductive material due to its extremely low conductivity of about 1×10^{-15} Sm^{-1}. Besides volume expansion during lithiation is another challenge of sulfur to be utilized in LIBs. Combining sulfur with reduced-graphene oxide(rGO) is shown to have better results mainly because rGO easily hosts the volume expansion of sulfur.[12] The composite cathode should also be ionically conductive. Combining rGO/Sulfur composites with ionically conductive solid electrolytes not only makes cathodes conductive but also decrease the chemical potential difference between the electrode and electrolyte.

In this study we report the successful synthesis of $Li_7P_3S_{11}$ solid electrolyte and assembling of an ASSLIB where Li_3N coated Li and sulfur active material composite served as anode and cathode, respectively. Chemical stability of Li_3N–$Li_7P_3S_{11}$ interfaces were studied by means of ab-initio molecular dynamics (AIMD) simulations.

Results and Discussion

Metastable glass-ceramic $Li_7P_3S_{11}$ phase synthesized by two step reaction where at first step stoichiometric amount of Li_2S-P_2S_5 powder mixture converted into glass form through ball-milling. Then, DSC analysis were carried out to reveal possible reactions during subsequent heat treatment to crystallize $Li_7P_3S_{11}$ phase from the obtained glassy powders. Figure 1 shows the XRD analysis of ball-milled and crystallized $Li_7P_3S_{11}$ phases along with DSC analysis in the inset. DSC analysis showed two exothermic peaks where each characterizes the crystallization of $Li_7P_3S_{11}$ and $Li_4P_2S_6$ phases. No other peaks was observed in the system up to 350 °C and glass transition temperature is observed at around 200 °C.

$Li_4P_2S_6$ phase formed according to the following reaction and shown to be having ionic conductivity on the order of 10^{-7} $S\,cm^{-1}$ at room temperature.[13,14] The structure is basically formed at temperatures higher than the crystallization temperature of $Li_7P_3S_{11}$ phase because of sulfur loss due to heat [Eq. (1)].

$$2Li_2S + P_2S_5 \rightarrow Li_4P_2S_6 + S \quad (1)$$

Raman analysis was carried out to observe the local environment of the $Li_7P_3S_{11}$ structure and the result given in Figure 2. Besides Raman analysis is a powerful technique to characterize the existence of impurity phases in the structure. Characterized peaks of $Li_7P_3S_{11}$ structure are observed at around 420,410 and 380 cm^{-1} where each peak stands for PS_4^{-3}, $P_2S_7^{-4}$and $P_2S_6^{-4}$. Small neck observed at around 380 cm^{-1} which stands for the existence of impurity $Li_4P_2S_6$ phase in trace amount.

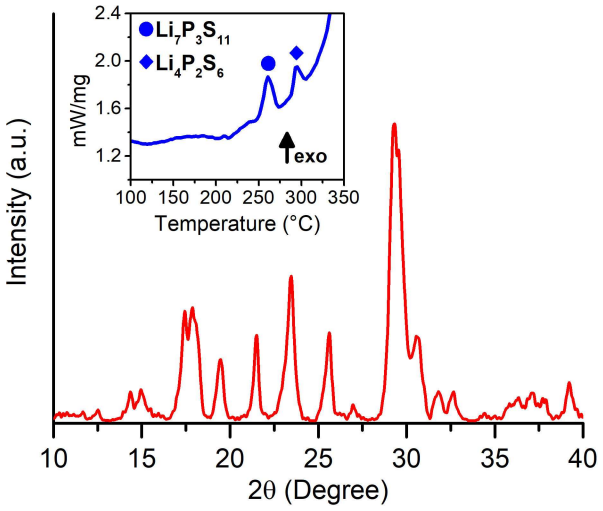

Figure 1. XRD analysis of $Li_7P_3S_{11}$ synthesis and DSC analysis (inset).

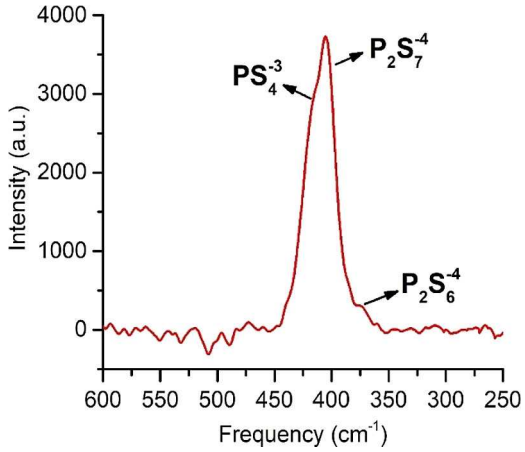

Figure 2. Raman analysis of synthesized $Li_7P_3S_{11}$.

Composite sulfur based rGO/S/CarbonBlack(CB)/$Li_7P_3S_{11}$cathode was utilized in assembled ASSLIB. Sulfur, CB and $Li_7P_3S_{11}$ was utilized as active, electronic and ionic conductive materials respectively. rGO utilized in the system to restrict the well-known volume expansion(contraction) of sulfur during lithiation(delithiation). Mixing active material with solid electrolytes decrease the chemical potential difference between the electrode and electrolyte so that side reactions were prevented in the system.

Figure 3 a shows the Raman analysis of rGO along with the XRD analysis of rGO in the inset. The well-known peak of GO at around 11° converted into peak at around 26° upon the reduction through heat treatment at 800 °C for 4 h under Ar-H_2

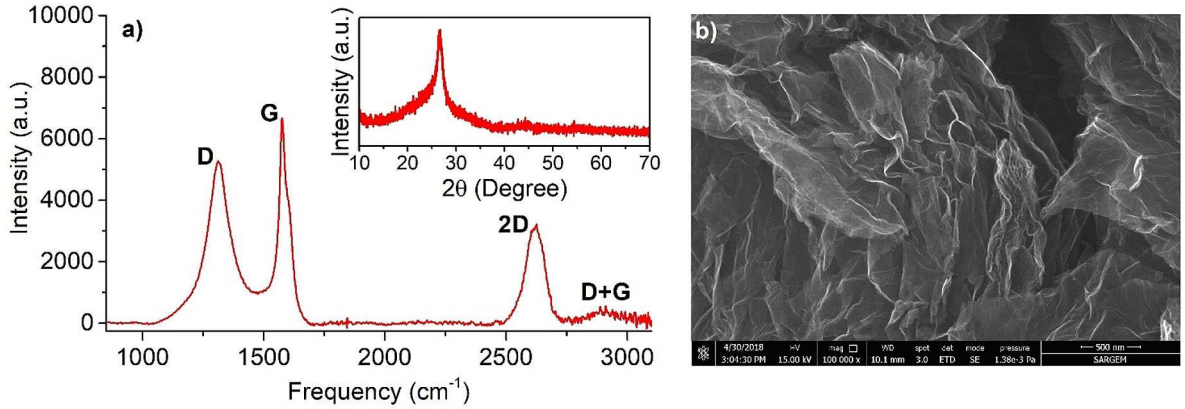

Figure 3. (a) Raman and XRD analysis of rGO and (b) morphology of the synthesized rGO.

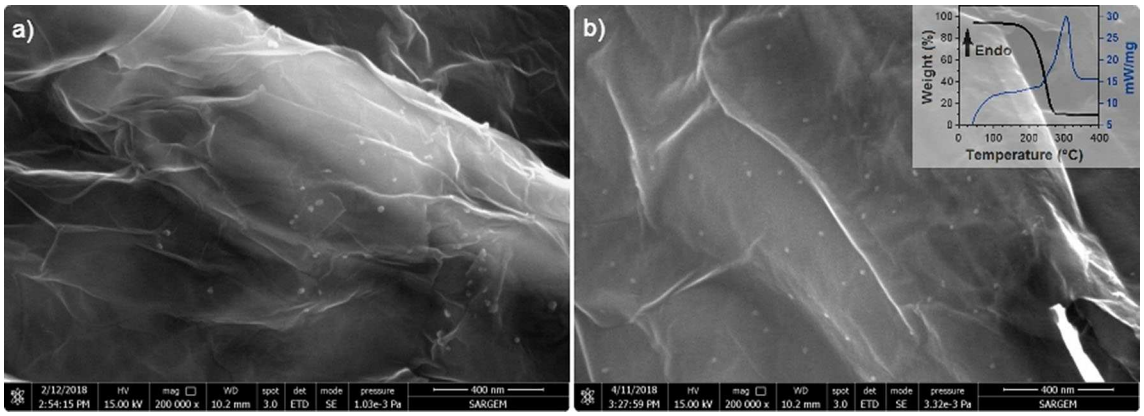

Figure 4. (a, b) FESEM images of rGO/S composite. Thermal gravimetry analysis of rGO/S composite (inset).

gas flow. In Raman analysis of obtained rGO structure, peak observed at around 1350 cm^{-1} indicates the structural defects and disorders named D band; where peak at around 1580 cm^{-1} denotes sp^2 hybridization of carbon atoms. Smaller D band compared to G band observed upon the reduction represents the less defective nature of the structure which yields better electronic conductivity in the cathode. Figure 3 b shows the well-known wrinkled morphology of synthesized rGO structure. Sulfur was added into rGO to prepare rGO/S composite. Figure 4 a–b shows the morphology of rGO/S composite. The tiny bits of particulates are the sulfurs impregnated into rGO matrix. They are well dispersed into the system and having sizes around 10 nm. The amount of sulfur soaked into rGO matrix was measured by Thermal Gravimetry and shown in the inset of Figure 4 b. The result shows that 85 percent of rGO/S composite composed of sulfur active material. Overall cathode composition contains sulfur active material as approximately 37.5 wt%.

TEM analysis was carried out to further analyze the interaction and distribution of rGO/S composite. As seen in Figure 5, sulfur particulates with the size of about 10 nm are well distributed within rGO which are expected to accommodate the expansion of sulfur during lithiation.

Li_3N layer was formed on the lithium anode chips through N_2 gas flow inside an air-tight reaction chamber at 50 °C.

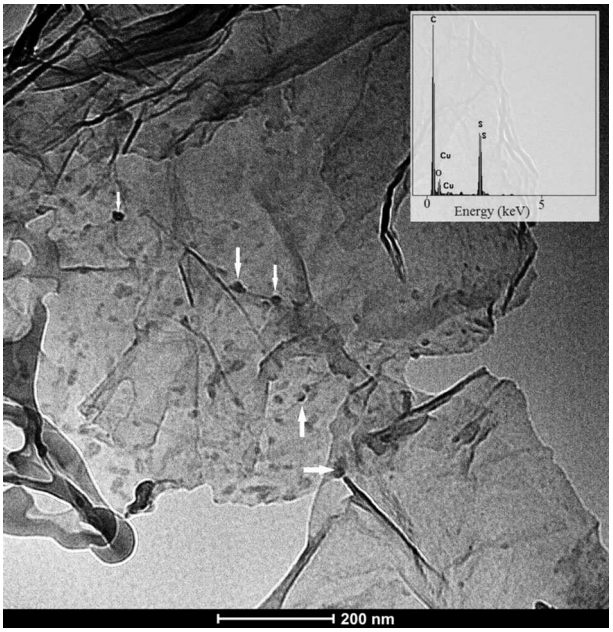

Figure 5. TEM analysis of rGO/S composite with EDS (inset).

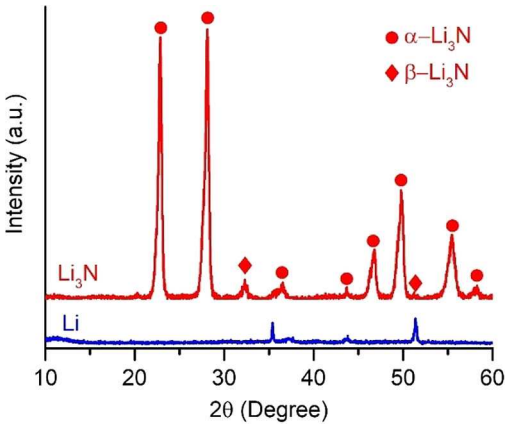

Figure 6. XRD analysis of pristine and Li_3N coated Li metal.

Figure 6 shows the XRD analysis of the Li_3N phase formed on the Li chips along with fresh Li chips. The peaks observed after nitridation assigned to α -Li_3N phase with JCPDF 30-0759 card. Tiny peaks at around 32° and 52° were assigned to β-Li_3N polymorphous arising due to the reaction at elevated temperature. Considering the low enthalpy barrier of α-Li_3N to β-Li_3N transition (0.01 eV)[8] it is inclined to get β-Li_3N polymorphous in synthesis at temperatures higher than room temperature.

Nitridation kinetics of lithium is abrupt due to the high reactivity of Li metal. Besides, native film existing at the surface oflithium foils consist of LiOH, Li_2O and Li_2CO_3[10] always affect the nitridation kinetics i.e. nucleation site of Li_3N phase Figure 7(a–b) shows the nitridation process taken during the synthesis where nitridation took place at the surface. Generally nitridation process starts withthe nucleation of Li_3N and proceeds through the depth of lithium metal instead of surface. Nucleation and kinetics of the new phase have to be controlled to get such kind of layer. Figure 7 c display the nitride layer formed on the surface of the lithium with the thickness of about 130 μm. As observed, contrary to lithium metal, Li_3N phase is hard and brittle.

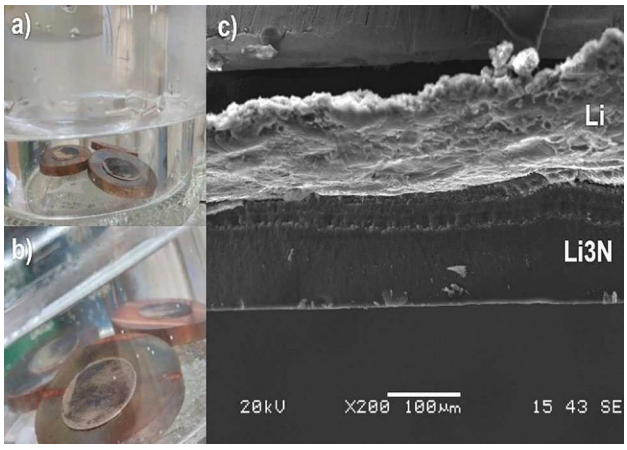

Figure 7. Synthesis of Li_3N layer on an Li anode where nitridation took place on the surface.

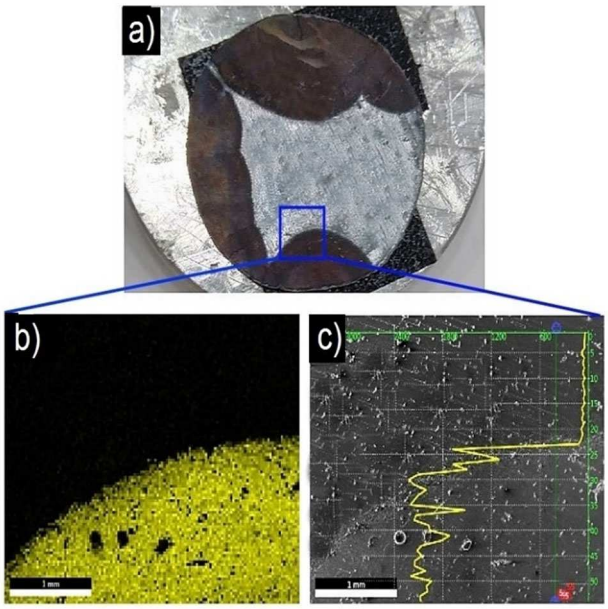

Figure 8. (a) Nitridation of Li metal where island growth observed. (b) EDS map and (c) line analysis of displayed rectangular area.

Figure 8 a shows the intermediate stage of nitridation process, where nitridation did not take place evenly on the surface. Figure 8 (b–c) shows the elemental and line mapping of the area shown within the rectangle on the Figure 8 a. On Figure 8 c, Upper(Darker) side of the image represents the un-nitrided part of the lithium where the other side(lighter) represents the nitrided part of the lithium. Line EDS analysis results(shown with yellow line) shows the nitrogen distribution on the nitrided and un-nitrided portion of the sample. The abrupt change in the nitrogen amount testifies the heterogeneous nitridation kinetics along with island-growth mechanism[7] of the synthesis. EDS dot mapping also testifies the uniform nitridation on the nitrided parts of the sample. The black dots observed in Figure 8b are oxide particulates formed during sample preparation due to exposure of air. Cracks were also liable to be formed on the nitrided part of the lithium chip due to the brittle nature of Li_3N phase.

To test the ionic conductivity of the prepared solid electrolyte ion-blocking In/$Li_7P_3S_{11}$/In symmetric cell were prepared. Figure 9 a shows the impedance measurement results where the inset displays the magnified high frequency semi-circle portion of the curve. Total ionic conductivity of the prepared solid electrolyte pellet is determined by the intercept between the x-axis and the straight line. Total conductivity of the pellet was measured as 4 mS cm^{-1} at room temperature. To test the electrochemical stability of the synthesized structure, we assembled Lithium/ $Li_7P_3S_{11}$/Stainless Steel cell. Only the peaks denote lithium stripping and deposition were observed in figure 9 b. The result shows that the synthesized structure has a wide electrochemical window up to at least 5 V. The electrochemical window of the cell were also tested in the system where Li anode replaced with Li_3N coated Li. Figure 9 c shows that Li_3N layer does not prevent lithium stripping and

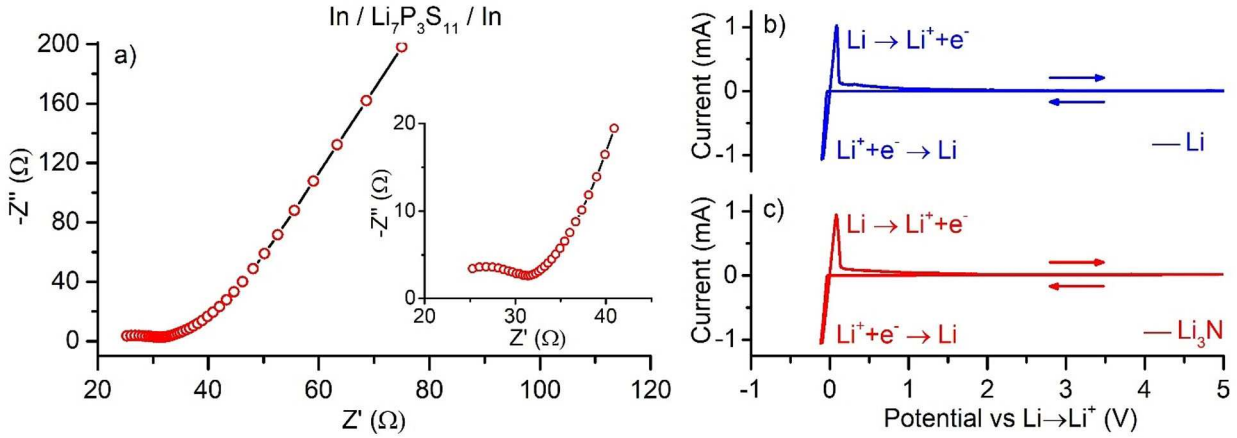

Figure 9. (a) Impedance analysis of synthesized $Li_7P_3S_{11}$ electrolyte in symmetrical cell. Inset shows the magnification of high frequency region. Electrochemical window of (b) Li and (c) Li_3N-protected Li assembled in $Li(Li_3N)/Li_7P_3S_{11}$/stainless steel cell.

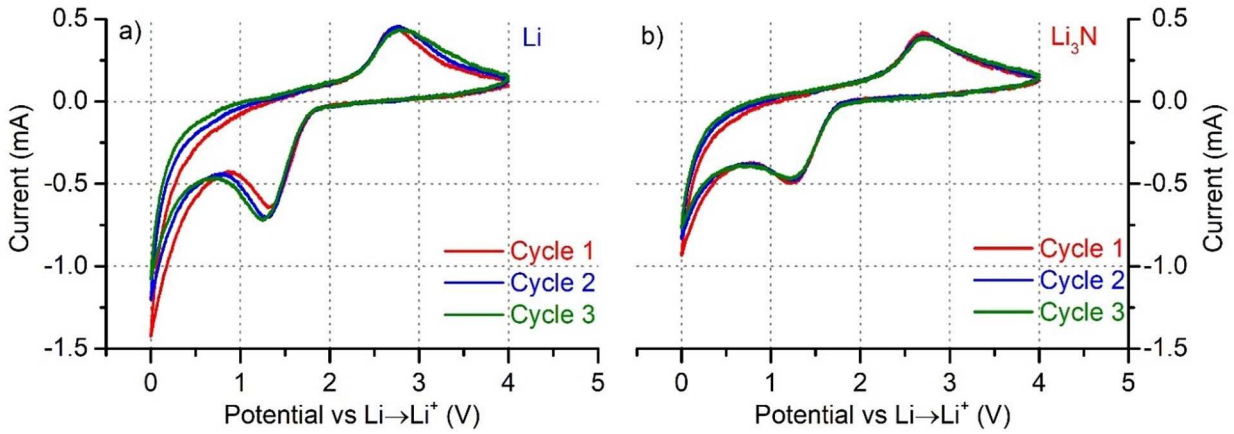

Figure 11. CV analysis of (a) $Li/Li_7P_3S_{11}/(rGO/S/CB/Li_7P_3S_{11})$ and (b) Li_3N coated $Li/Li_7P_3S_{11}/(rGO/S/CB/Li_7P_3S_{11})$ cell.

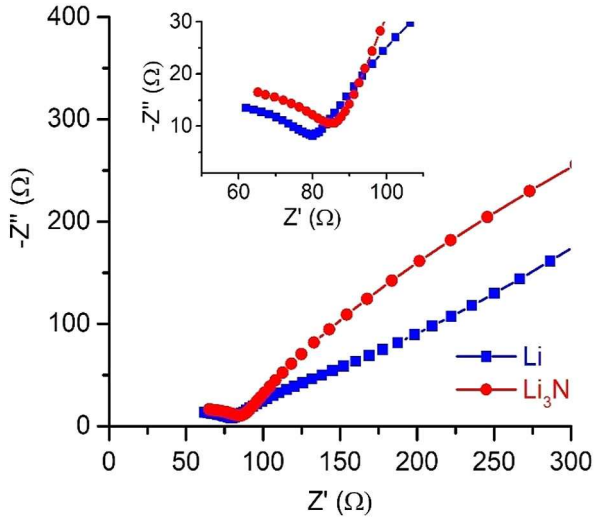

Figure 10. Impedance analysis of the cell with pure lithium and Li_3N protected Li used as anode where $Li_7P_3S_{11}$ and $(rGO/S/CB/Li_7P_3S_{11})$ used as solid electrolyte and cathode respectively.

deposition in the cell. Beside any reaction due to Li_3N was not observed in system up to 5 V.

Figure 10 shows the impedance measurements conducted on Li(or Li_3N)$/Li_7P_3S_{11}/$(S-rGO-CB-$Li_7P_3S_{11}$) systems. Both cells have about the same total impedance(bulk + grain boundary resistance) which shows that Li_3N layer does not contribute to total impedance of the system mainly due to high ionic conductivity and thin layer ofLi_3N phase.

Asymmetric Li (or Li_3N)$/Li_7P_3S_{11}/$(S-rGO-CB-$Li_7P_3S_{11}$) cell constructed to evaluate the reduction and oxidation reactions of the sulfur based cathode composite. The results given in Figure 11 show that two peaks representing $S + 2Li^+ + 2e^- \rightleftharpoons Li_2S$ reactions observed in both systems as common in all-solid state batteries utilizing sulfur as cathode active material. Anodic peak representing the oxidation of Li_2S to lower order polysulfides observed at around 2.8 V vs Li/Li^+. Cathodic peak representing the reduction of sulfur to higher order polysulfides observed at around 1.3 V vs Li/Li^+ at first cycle. Difference between anodic and cathodic peaks were found to be increasing with cycling on pure Li anode system indicating that

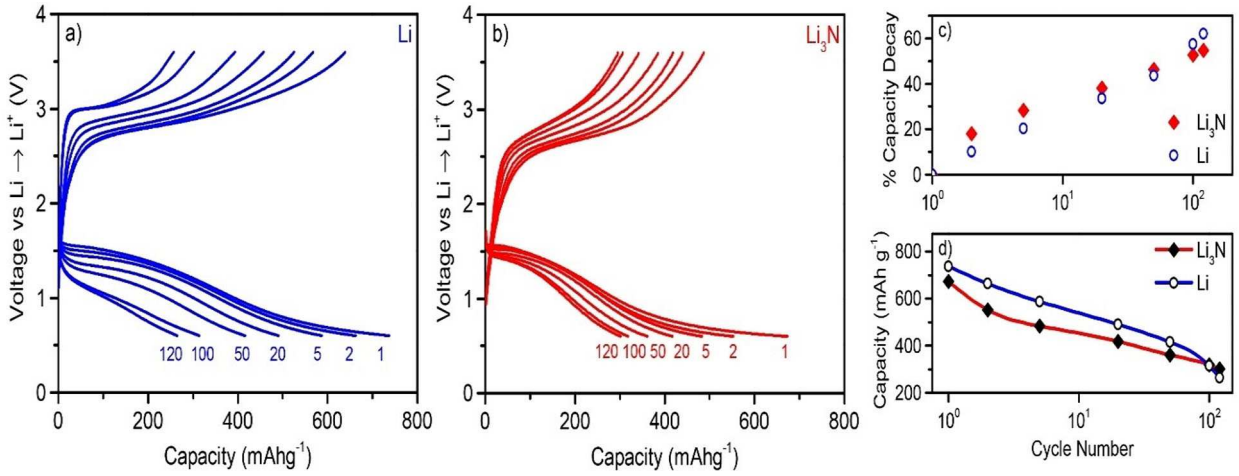

Figure 12. Cyclic performance of(a) Li/$Li_7P_3S_{11}$/(rGO/S/CB/ $Li_7P_3S_{11}$) (b) Li_3N coated Li/$Li_7P_3S_{11}$/(rGO/S/CB/ $Li_7P_3S_{11}$) cell at 25 °C. (c) Capacity decay upon cycling with respect to initial capacity. (d) Capacity of the cells upon cycling.

polarization is increasing in the system. Whereas on Li_3N coated Li anode system polarization were not increased upon cycling.

Galvanostatic cyclic charge-discharge tests conducted between 0.6–3.6 V (vs Li/Li^+) at a current density of 160 mAg^{-1} and the results given in Figure 12 (a–b). Contrary to Li–S batteries with liquid electrolytes where two plateau observed due to the production of polysulfide intermediates, here, in solid electrolytes we observed one charge an discharge plateau as the only electrochemical reaction governing the reaction is $S + 2Li^+ + 2e^- \rightleftharpoons Li_2S$. Cycling tests reveal that cell assembled with pure lithium anode delivers higher initial capacities. However upon cycling capacity degradation is lower on the cell assembled with Li_3N protected lithium anode. Cell with pure lithium anode has initial and final capacities of 730 and 260 $mAh\,g^{-1}$ after 120 cycles whereas cell with Li_3N coated lithium anode has initial and final capacities of 680 and 306 $mAh\,g^{-1}$. Figure 12 c display the capacity decay upon cycling with respect to initial capacity of both cells. Capacity decay is lower on Li_3N protected system. Figure 12 d display the capacity of the cell with respect to cycle number. Cell with pure lithium anode has higher capacity until 75 cycles, yet the capacity of the cell with Li_3N protected anode is higher afterwards.

Conclusion

In summary, $Li_7P_3S_{11}$ solid electrolyte is successfully synthesized and utilized in an ASSLIB where anode compose of Li_3N coated Li metal and cathode is a quaternary sulfur based composite. The analysis on the effect of Li_3N coating on Li metal anode revealed that the layer does not impede charge transfer substantially. Therefore, Li_3N coating can be utilized in ASSLIBs to prevent the corrosion of Li anode in contact with solid electrolyte. Besides facile synthesis route of Li_3N makes such kind of coatings feasible for mass production. Our molecular dynamic analysis revealed that $Li_7P_3S_{11}$ solid electrolyte does not degrade in contact with Li_3N within our 1.2 ps simulation. To our best knowledge there is not any study relating the use of Li_3N coated Li anode at ASSLIBs and our results present promising characteristics of Li_3N to improve the cycle ability of Li-ion batteries.

Experimental Section

$Li_7P_3S_{11}$ Synthesis

$Li_7P_3S_{11}$ glass ceramic powders were synthesized by ball milling and subsequent heat treatment of Li_2S (99.98%, Sigma Aldrich) and P_2S_5 (99%, Merck) powders. Stoichiometric amount of powders were put into zirconia pot with 16 balls (10 mm) and rotated at 400 rpm for 24 h intermittently to prevent any sulfur loss due to heat. Ball milled glassy powders were then put into sealed quartz tube and sintered at 265 °C for 2 h. All synthesis procedure was carried out in glovebox (MBRAUN LABstar) to prevent the exposure of powders to air.

Phase analysis of synthesized powders were carried out by X-ray diffraction (Rigaku D/MAX 2000) with Kapton band sealed apparatus. Raman analysis was utilized to observe the local environment of the synthesized $Li_7P_3S_{11}$ structure with 732 nm laser. DSC analysis was carried out prior to crystallization heat treatment to characterize the possible exo(endo)thermic reactions during synthesis.

rGO/S/CB/$Li_7P_3S_{11}$ Composite Cathode Synthesis

Quaternary cathode composition utilized in this study. Graphene oxide(GO) powders, synthesized by modified Hummers method, were heat treated at 800 °C for 4 h in Ar-H_2 atmosphere to convert GO into reduced Graphene Oxide(rGO). Exfoliated rGO structure were then mixed withas-dried sulfur in sealed quartz tubes at 155 °C for 12 h [(rGO):S 1:5 wt%] to penetrate sulfur into rGO. Obtained composite were then mixed with SuperP as electronic conductive agent at cathode by ball milling at 370 rpm for 8 h [(rGO:S):SuperP 3:1 wt%]. Last step of cathode production was composed of mixing rGO-S-SuperP composite with $Li_7P_3S_{11}$ powders by ball milling at 370 rpm for 8 h [(rGO:S:SuperP):$Li_7P_3S_{11}$60:40 wt %].

Li_3N Coated Li Anode Synthesis

Nitride coating of anode surface was carried out by ex-situ nitridation method where N_2 gas allowed to flow through lithium chip containing sealed reaction chamber. Lithium chips with 300 μm thickness were initially scratched by a scalpel to clean surface films and then exposed to N_2 gas(99.999% purity) flow with 100 sccm for 2 h at 50 °C. Li_3N layer first nucleates at the surface of the chipand then depending on the kinetics of the reaction proceeds either toward surface or depth of the chip.Black colored Li_3N thin film formed on the lithium surface were then characterized by elemental and phase composition utilizing FESEM and X-ray Diffraction respectively.

Li_3N layer was confined only to the surface of Li metal to take advantage of the higher theoretical capacity of lithium (3862 mAh g^{-1}) instead of Li_3N. Besides pure Li_3N phase is brittle so that in all solid state batteries, where pressure is applied, it can be utilized in powder form. However, density and contact problems will unavoidably be faced in this case.

Electrochemical Tests

Electrochemical tests were conducted at GAMRY(Gamry Instruments Reference 1000)workstation. Synthesized solid electrolyte powders of about 90 mg were put into a PEEK insulated die (10 mm dia.) and pressed under 400 Mpa. 4 mg cathode powders corresponding to 1.175 mg cm^{-2} active material loadwere then spread onto the $Li_7P_3S_{11}$ pellet and pressed under 340 MPa. At last, lithium chip was placed onto the other side of the pellet and pressed under 120 MPa. Stainless steel punches were utilized as pressure transmitting media along with current collectors in the cell. Impedance tests were carried out with symmetrical In/$Li_7P_3S_{11}$/In cell at frequency between 1 MHz–1 Hz with 10 mV amplitude. Cyclic Voltammetry(CV) tests were conducted by asymmetrical Li/$Li_7P_3S_{11}$/Stainless Steel cell between −0.2–5 V (vs Li/Li^+) with 1 mV/s step size to evaluate the electrochemical window of the synthesized solid electrolyte. CV tests were also carried out atLi(or Li3 N)/$Li_7P_3S_{11}$/(S-rGO-CB-$Li_7P_3S_{11}$) cells between 0–4 V to observe the anodic and cathodic reactions in the cell with 1 mV/s stepsize. Galvanostatic electrochemical charge-discharge tests were conducted between 0.6–3.6 V (vs Li/Li^+) with a current density of 160 mA g^{-1}. Capacity was calculated according to the amount of sulfur active material in the cathode.

Molecular Dynamic Simulations

Ab-initio molecular dynamics(AIMD) simulations were performed using Vienna Ab initio Simulation Package(VASP)[16,17] to mimic the Li_3N-$Li_7P_3S_{11}$ interface. Perdew-Burke-Ernzerhof (PBE) version of Projected augmented wave (PAW) pseudopotentials were utilized. Energy cutoff of 400 eV used within gamma centered 1×1×1 k-point. Time-step were selected as 1 fs with 1200 timestep to get 1.2 ps length simulation. Simulation time kept short due to computational costs. $Li_7P_3S_{11}$ with triclinic crystal structure lack of having symmetry. Therefore it is extremely challenging to construct compatible interface between triclinic $Li_7P_3S_{11}$ (Space group = P1) and hexagonal Li_3N (Space group = P_6/mmm(191)) within reasonable number of atoms for molecular dynamics studies. To construct interface with Li_3N phase we selected the atoms reside within the enclosed rectangular prism of trigonal $Li_7P_3S_{11}$ structure which does not preserve the stoichiometry. $Li_{46}P_{24}S_{78}$ structureutilized in this study which deviates from the seven fold supercell structure of $Li_7P_3S_{11}$ by−6.2%,−14.3% and 1.3% for Li, P and S respectively. Therefore our model utilized to resemble the interface is lack of lithium and excess of sulfur and phosphorus. For Li_3N side we constructed interface by trimming from supercell so that the interface has dimensions 16.97 Å and 12.35 Å in z and y directions with the thickness of 8.91 Å.

Acknowledgements

This work was supported by Research Fund of the Sakarya University under the project no: 2017-01-08-043

Conflict of Interest

The authors declare no conflict of interest.

Keywords: all-solid-state batteries · electrochemistry · electrodes · lithium nitride · solid electrolytes

[1] N. Kamaya, K. Homma, Y. Yamakawa, M. Hirayama, R. Kanno, M. Yonemura, T. Kamiyama, Y. Kato, S. Hama, K. Kawamoto, A. Mitsui, *Nat. Mater.* **2011**, *10*, 682–686.
[2] P. Bron, B. Roling, S. Dehnen, *J. Power Sources* **2017**, *352*, 127–134.
[3] C. Yu, L. van Eijck, S. Ganapathy, M. Wagemaker, *Electrochim. Acta* **2016**, *215*, 93–99.
[4] Y. Seino, M. Nakagawa, M. Senga, H. Higuchi, K. Takada, T. Sasaki, J. *Mater. Chem.* **2015**, *3*, 2756–2761.
[5] S. Wenzel, D. A. Weber, T. Leichtweiss, M. R. Busche, J. Sann, J. Janek, *Solid State Ionics* **2016**, *286*, 24–33.
[6] Y. Zhu, X. He, Y. Mo, *Adv. Sci.* **2017**, *4*, 1600517.
[7] Y. J. Zhang, W. Wang, H. Tang, W. Q. Bai, X. Ge, X. L. Wang, C. D. Gu, J. P. Tu, *J. Power Sources* **2015**, *277*, 304–311.
[8] G. Ma, Z. Wen, M. Wu, C. Shen, Q. Wang, J. Jin, X. Wu, *Chem. Commun.* **2014**, *50*, 14209–14212.
[9] K. Park, J. B. Goodenough, *Adv. Energy Mater.* **2017**, *7*, 1700732.
[10] Y. Sun, Y. Y. Li, J. Sun, Y. Y. Li, A. Pei, Y. Cui, *Energy Storage Mater.* **2017**, *6*, 119–124.
[11] M. Baloch, D. Shanmukaraj, O. Bondarchuk, E. Bekaert, T. Rojo, M. Armand, *Energy Storage Mater.* **2017**, *9*, 141–149.
[12] R. Xu, Z. Wu, S. Zhang, X. Wang, Y. Xia, X. Xia, X. Huang, J. Tu, *Chem. Eur. J.* **2017**, *23*, 13950–13956.
[13] Z. D. Hood, C. Kates, M. Kirkham, S. Adhikari, C. Liang, N. A. W. Holzwarth, *Solid State Ionics* **2016**, *284*, 61–70.
[14] L. E. Rush, N. A. W. Holzwarth, *Solid State Ionics* **2016**, *286*, 45–50.
[15] T. Cheng, B. V. Merinov, S. Morozov, W. A. Goddard, *ACS Energy Lett.* **2017**, *2*, 1454–1459.
[16] G. Kresse, D. Joubert, *Phys. Rev. B* **1999**, *59*, 1758–1775.
[17] G. Kresse, J. Furthmüller, *Phys. Rev. B* **1996**, *54*, 11169–11186.

Manuscript received: October 22, 2018
Revised manuscript received: January 21, 2019
Accepted manuscript online: January 23, 2019